Photoelectron-momentum distribution of H_2^+ molecules at different internuclear distances in an elliptically polarized laser field

Hong-Dan Zhang, Shuai Ben, Tong-Tong Xu, Kai-Li Song, Yan-Rong Tian, Qing-Yun Xu, Si-Qi Zhang, Jing Guo,* and Xue-Shen Liu†

Institute of Atomic and Molecular Physics, Jilin University, Changchun 130012, People's Republic of China

(Received 4 April 2018; published 30 July 2018)

We investigate molecular photoelectron-momentum distribution (MPMD) and molecular photoelectron angular distribution (MPAD) of oriented H_2^+ under frozen-nuclei approximation driven by elliptically polarized laser pulse by numerically solving a two-dimensional time-dependent Schrödinger equation. The results show that the MPMDs and MPADs are sensitive to the internuclear distance, which is illustrated by the initial MPMDs and the evolution of MPMDs. In addition, they are also dependent on laser ellipticity and wavelength. When the laser wavelength is 5 nm, the phenomenon of laser-induced electron diffraction can be observed in both MPMD and MPAD.

DOI: 10.1103/PhysRevA.98.013422

I. INTRODUCTION

Rapid advances of ultrashort laser pulses offer the potential for imaging and steering of electronic dynamics which normally occurs on the femtosecond (1 fs $= 10^{-15}$ s) timescale [1–4]. The pump-probe technique has been widely employed in real-time imaging in electronic dynamics [5,6]. The target is hit by the ultrashort pump pulse initiating a transition, and the dynamics of the target is monitored by probe pulse after a variable delay time.

Some advanced research employing the pump-probe technique has attracted much attention such as laser Coulomb explosion imaging [7] for nuclear motion and laser-induced electron diffraction (LIED) [8–10] for coupled electron-nuclear motion. The core of diffraction is to image or probe the time-resolved structure of molecules on attosecond (1 as $= 10^{-18}$ s) time resolution and subnanometer resolution. And it would be very useful in the study of chemical and biochemical processes.

Recently, a single pulse with 53 as duration has been achieved by Li *et al.* [11] utilizing intense two-cycle driving pulses near 1.8 μm center wavelength. The shortest single attosecond soft-x-ray pulse of 43 as is obtained by Gaumnitz *et al.* [12], which provides a better tool tracking electronic dynamics regardless of the interaction from nuclear motion.

The photoelectron-momentum distribution (PMD) as well as photoelectron angular distribution (PAD) originating from the ionization of atoms and molecules by intense laser pulses convey valuable and fruitful information about the electronic and nuclear structure of the target. Different PMD parts reflect different aspects of the ionization dynamics and encode different target structure information and the physical mechanism deep inside.

The atomic PMD has been investigated under midinfrared (MIR) or extreme ultraviolet (XUV) laser theoretically. Murakami and Chu [13] exemplified the mechanism of symmetry breaking in PMD of a hydrogen atom. The information of different ionization pathways of He^+ is encoded in photoelectron spectra; both the relative phase between two XUV lasers and the intensity of the XUV pulse have an effect on the final PMD [14]. Yuan *et al.* [15,16] demonstrated the dependence of molecular photoelectron-momentum distribution (MPMD) on the molecular orbital symmetry. In addition, the interference between direct ionized electrons and rescattered electrons also had an effect on the MPMD.

Experimentally, the research on PMD for deep structural mechanisms and dynamics of atoms and molecules is also continuing [17–21]. In order to get a deeper understanding of the neon atom, Villeneuve *et al.* [17] experimentally disentangled the angular momentum components by a train of attosecond pulses synchronized with an infrared laser field. Odenweller *et al.* [21] studied the electron emission from the H_2^+; the complex laser-driven electron dynamics is encoded in the unexpected momentum distribution.

With the development of the ultrafast attosecond laser [2], one can rely on LIED [8] to illuminate the target more clearly. Cohen and Fano [22] have predicted such interference phenomena in diatomic molecules earlier in perturbative single-photon ionization, which has been extended to nonperturbative photoionization in LIED later [8]. The subsequent research on LIED is still continuing [9,10,23–25].

Attosecond XUV laser pulses have gradually become a promising tool to study the ultrafast phenomena. The high harmonic generation (HHG) assisting with relative low intensity XUV is studied to illuminate the precise dynamics behavior of electrons [26,27]. XUV with extremely low intensity has been employed to launch the coherent XUV amplification of HHG from the helium atom [28]. Cui *et al.* [29] investigated the PMD originating from a hydrogen atom exposed to the MIR and XUV pulse, and the PMD can be precisely tailored. In addition, it shows that the interference pattern can be applied to extract the carrier envelope phase of an attosecond pulse, which is a promising way to witness the subcycle dynamics.

*gjing@jlu.edu.cn
†liuxs@jlu.edu.cn

Further, few-cycle attosecond XUV pulses have also attracted attention for tailoring electronic motion [30,31]. Yuan *et al.* [32] compared the interference effects of the molecular orbital of H_2 and H_2^+ in two-dimensional (2D) LIED by XUV laser pulses.

In this paper, we present numerical results of MPMD and molecular photoelectron angular distribution (MPAD) of aligned H_2^+ under an elliptically polarized laser pulse. The results show that the MPMDs and MPADs are dependent on laser ellipticity and internuclear distance. When the laser wavelength is changed from 35 to 5 nm, the phenomenon of LIED can be observed in both MPMD and MPAD. Both the attosecond perturbation ionization theory and the exactly solvable photoionization model are adopted to interpret the results.

The paper is arranged as follows: In Sec. II, we briefly introduce our theoretical model and computational method. In Sec. III, we present computational results for different cases. Finally, a summary is given in Sec. IV. Atomic units ($e = m_e = \hbar = 1$) are used throughout, unless specified otherwise.

II. THEORETICAL MODEL AND NUMERICAL METHOD

We consider a fixed nuclei x-aligned H_2^+ exposed to the elliptically polarized laser field. The 2D time-dependent Schrödinger equation (TDSE) under frozen-nuclei approximation can be given by

$$i\frac{\partial\phi(x,y,t)}{\partial t} = \left[\frac{p_x^2+p_y^2}{2} + V(x,y) + xE_x(t) + yE_y(t)\right]\phi(x,y,t). \tag{1}$$

The soft-core Coulomb potential can be expressed as

$$V(x,y) = -\frac{1}{\sqrt{(x-R/2)^2+y^2+c}} - \frac{1}{\sqrt{(x+R/2)^2+y^2+c}}, \tag{2}$$

where R is the internuclear distance, and $c = 0.5$ is the soft-core parameter ($R = R_e = 2$ a.u. is the equilibrium internuclear distance; the selected parameters R_e and c correspond to the first ionization energy -1.1 a.u. for H_2^+). $E_x(t)$ and $E_y(t)$ are the x and y components of the laser field, and p_x and p_y are the momentum of electrons in the x and y directions. The total time-dependent potential is

$$U(x,y,t) = V(x,y) + xE_x(t) + yE_y(t). \tag{3}$$

The 2D TDSE is solved by means of the splitting-operator fast-Fourier transform technique. The initial wave packet is constructed by the imaginary time-propagation method. And the wave function at any time can be expressed as

$$\phi(x,y,t_0+\Delta t) = e^{-i[(p_x^2+p_y^2)/4]\Delta t}e^{-iU(x,y,t)\Delta t}e^{-i[(p_x^2+p_y^2)/4]\Delta t} \times \phi(x,y,t_0) + O(\Delta t)^3. \tag{4}$$

The length of the integration grid is 409.6 a.u. The wave function is multiplied by a $\cos^{1/8}$ mask function at each time step to prevent unphysical effects originating from the reflection of the wave packet from the boundary. And the domain of absorption ranges from $|x, y| = 150$ a.u. to $|x, y| = 204.8$ a.u. When the wave function propagates to the final time, the ionization part is recorded as $[1 - M(r)]\phi(x, y, t_f)$, $\phi(x, y, t_f)$ is the wave packet at final time, and $r = \sqrt{x^2+y^2}$, the mask function is

$$M(r) = \begin{cases} 1, & r \leqslant r_b \\ \exp[-\beta(r-r_b)], & r > r_b, \end{cases} \tag{5}$$

where $\beta = 1$ a.u., and the boundary for ionized wave function and bounded wave function is set to be $r_b = 20$ a.u. [33]. The MPMD can be obtained by Fourier transforming the ionized wave function into momentum space. For the calculations here, the time duration lasts for ten optical cycles, and the time propagation is continued for another four optical cycles to allow for some time to relax. The MPAD is obtained from the MPMD.

III. RESULTS AND DISCUSSION

We first investigate elliptically polarized attosecond UV photoionization of aligned H_2^+ (at equilibrium $R_e = 2$ a.u.). The elliptically polarized driving laser field in our simulation is

$$\mathbf{E}(t) = E_x(t)\hat{\mathbf{e}}_x + E_y(t)\hat{\mathbf{e}}_y = E_0 f(t)\left[\frac{1}{\sqrt{1+\varepsilon^2}}\cos(\omega t)\hat{\mathbf{e}}_x + \frac{\varepsilon}{\sqrt{1+\varepsilon^2}}\sin(\omega t)\hat{\mathbf{e}}_y\right], \tag{6}$$

where $E_0 = 0.12$ a.u. ($I_0 = 5\times10^{14}$ W/cm^2) is the amplitude of the laser field, ε is the ellipticity constant, ω is the angular frequency of the laser field, and $\hat{\mathbf{e}}_{x/y}$ is the laser polarization direction. The laser pulse envelope $f(t) = \sin(\pi t/\mathrm{nT})^2$ is employed, $n = 10$, and $T = 2\pi/\omega$ is the optical cycle of the pulse.

Figure 1 shows the MPMDs and MPADs of H_2^+ with varying ellipticity. The pulse wavelength $\lambda = 30$ nm ($\omega = 1.52$ a.u.) is chosen in the calculation. In the current simulation, the ionization of molecules can occur by absorbing only one photon ($\omega > I_p$) which is the single-photon process. The ellipticity of the driving laser field is 0.25 [Figs. 1(a1) and 1(a2)], 0.5 [Figs. 1(b1) and 1(b2)], 0.75 [Figs. 1(c1) and 1(c2)], and 1 [Figs. 1(d1) and 1(d2)], respectively.

It can be seen that MPMDs are localized mainly along the y axis with a small angle which mainly comes from the resulting effects of the nonspherical molecular Coulomb potential and the helicity of the laser field with tilting in the same direction as the rotation of the laser field [21,34]. The previous experimental research in IR [21] and UV [35] regimes under a circularly polarized laser field exhibit the same phenomenon in MPMD. Such phenomenon can be observed in subsequent theoretical research in a circularly polarized laser field [16,33].

In our simulation, the results under the circularly polarized laser field (30 nm, 5×10^{14} W/cm^2) in Fig. 1(d1) presents a similar distribution pattern to that of the experimental results under the circularly polarized laser field (800 nm, 6×10^{14} W/cm^2) shown in Fig. 1(e) in Ref. [21]. In addition,

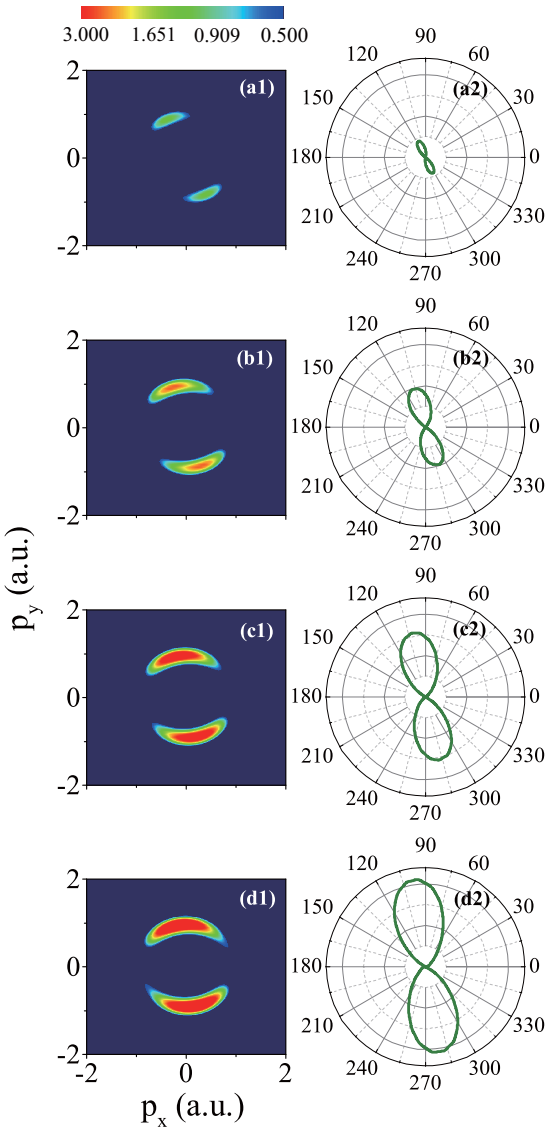

FIG. 1. The 2D MPMDs and MPADs of aligned H_2^+ at equilibrium $R_e = 2$ a.u. by elliptically polarized laser pulse ($\lambda = 30$ nm). The molecule is aligned along the x axis. The ellipticity in (a1) and (a2), (b1) and (b2), (c1) and (c2), and (d1) and (d2) is $\varepsilon = 0.25$, 0.5, 0.75, and 1, respectively. The left column is MPMDs and the right column is MPADs.

the results under an elliptically polarized laser field here also exhibit a similar distribution pattern to that in Ref. [21]. And the distributions become much wider and intense along with the increasing ellipticity.

The laser parameters here are the same as those in Ref. [16], and the MPMDs shown in Fig. 1 are similar to that in Ref. [16] except for the direction of rotation. That is because the laser field in our simulation is the left-handed polarized pulse, while the laser field in Ref. [16] is the right-handed polarized pulse, and the MPMDs tilt in the same direction as the rotation of the electric field vector in the laser pulse.

The attosecond perturbation ionization theory [36,37] and exactly solvable photoionization model of H_2^+ using the δ-function pulse [8,16,38] can be employed to interpret the results (see Ref. [16] for details).

We can see from Eqs. (11) and (12) in Ref. [16] that the maximum distribution of MPMDs meets the condition $\cos^2(\mathbf{p}\cdot\mathbf{R}/2) = \cos^2[pR\cos(\theta)/2] = 1$ which means that $\cos(\theta) = 0$, thus $\theta = n\pi + \pi/2$, $n = 0, \pm1, \pm2, \ldots$, where θ is the angle between the ionized electron and the axis of the molecule, i.e., the x axis. Thus, the photoionization distributions are mainly localized along the y axis and the interference term in Eq. (12) in Ref. [16] could be almost neglected since the value of $\sin(2\theta)$ is nearly zero. The distribution along the y direction can be obtained by computing the module square of transition amplitude along the y direction in Eq. (11) in Ref. [16],

$$\left|A_{\sigma_g}^{(y)}\right|^2 \propto 2|\eta^{(y)}|^2 E_y^2 \sin^2(\theta)\cos^2[(\mathbf{p})\cdot\mathbf{R}/2]\psi_{1s}^2(|\mathbf{p}|). \quad (7)$$

When the ellipticity is changed, the distribution along the y direction is positively correlated with the value of $\varepsilon^2/(1+\varepsilon^2)$ which is included in E_y^2. The numerical values of $\varepsilon^2/(1+\varepsilon^2)$ are respectively 0.06, 0.20, 0.36, and 0.50 when ε is 0.25, 0.50, 0.75, and 1, respectively. The increasing $|A_{\sigma_g}^{(y)}|^2$ presents the stronger distribution along the y direction, which well explains the MPMDs in Figs. 1(a1)–1(d1).

Figures 1(a2)–1(d2) show the MPADs with increasing ellipticity. The length of radius represents the intensity of the MPAD. As can be seen, the radius of MPAD becomes larger as the laser ellipticity increases. In addition, the angle of distributions respectively cover about 10°, 20°, 45°, and 50°, showing the broader distribution along with the increasing ellipticity, which is in good agreement with that in Figs. 1(a1)–1(d1).

In order to further understand MPMDs of molecules, the R dependence of MPMDs is shown in Fig. 2. The ellipticity of the driving laser field is fixed at $\varepsilon = 0.5$. The internuclear distance is $R_1 = 1.9$ a.u. [Figs. 2(a1) and 2(a2)], $R_2 = R_e = 2$ a.u. [Figs. 1(b1) and 1(b2)], $R_3 = 2.1$ a.u. [Figs. 2(b1) and 2(b2)], and $R_4 = 2.2$ a.u. [Figs. 2(c1) and 2(c2)], respectively.

Note that the length of the MPAD lobe in Fig. 1 represents the intensity of MPMD, and the intensity is increasing gradually with the increasing ellipticity of the laser pulse, thus the lobe of MPAD is larger and larger in the current unified scale [Figs. 1(a2)–1(d2)]. In Figs. 2(a2)–2(c2), another appropriate unified scale is chosen in the research of sensitivity on internuclear distance. That is the reason why the size of the MPAD for $R = R_e = 2$ a.u. in Fig. 1(b2) seems smaller than that in Figs. 2(a2)–2(c2). In addition, the soft-core parameters chosen for different internuclear distances are the same, which is due to approximately the same ionization energy calculated under R_1, R_3, and R_4 compared to that under R_e. Other parameters remain the same as that in Fig. 1.

The small tilted angle relative to the y axis in MPMDs and MPADs mainly comes from the effect of the Coulomb potential [21,34] and the helicity of the laser field. The dependence of the distribution pattern on the internuclear distance can be traced in Figs. 1(b1) and 1(b2) and 2. As the internuclear distance increases, no substantial change is observed in the MPMD along the y axis, while the end spots in the distribution along the x axis become more and more intense. The tendency can also be seen in MPADs in Figs. 1(b2) and 2(a2)–2(c2).

To have a better understanding on the sensitivity of MPMDs on internuclear distance, the initial MPMDs under different internuclear distances, which are obtained by imaginary

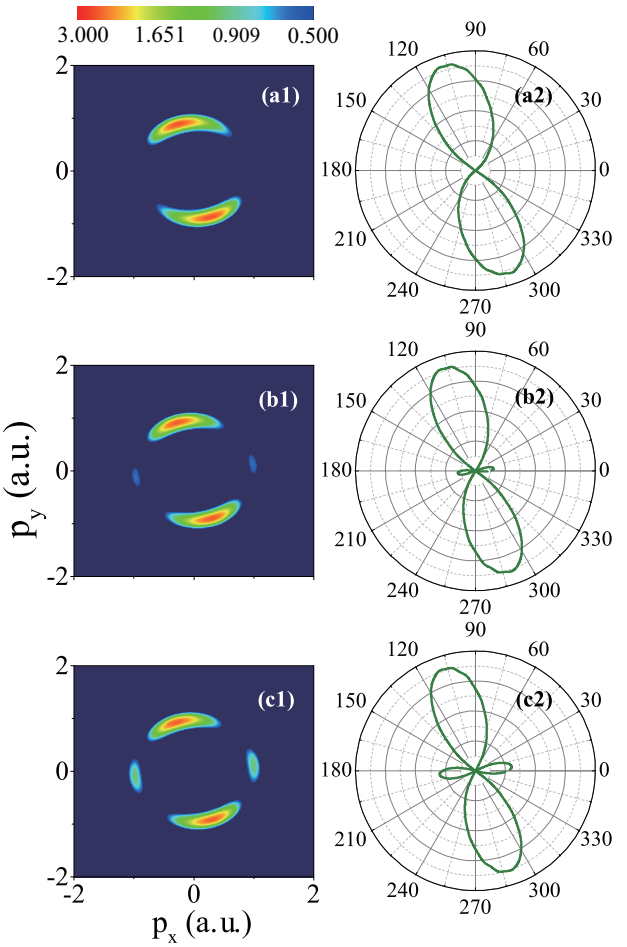

FIG. 2. The 2D MPMDs and corresponding MPADs of aligned H_2^+ by elliptically polarized laser pulse ($\lambda = 30$ nm, $\varepsilon = 0.5$) with changing internuclear distance. The molecule is aligned along the x axis. The internuclear distance in (a1) and (a2), (b1) and (b2), and (c1) and (c2) is $R = 1.9$, 2.1, and 2.2 a.u., respectively. The left column is MPMDs ane the right column is MPADs.

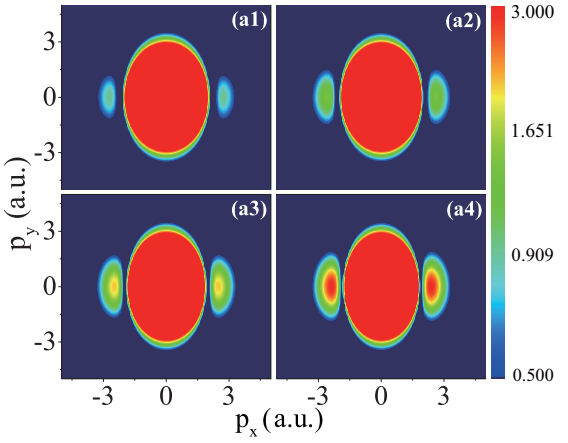

FIG. 3. The initial 2D MPMDs under (a1) $R = 1.9$ a.u., (a2) equilibrium $R_e = 2$ a.u., (a3) $R = 2.1$ a.u., and (a4) $R = 2.2$ a.u., respectively.

Let us consider the evolution of MPMDs at some R, taking $R_2 = R_e = 2$ a.u., for example, at $t = 3.6$ optical cycles, the MPMD [Fig. 4(a2)] localize along the y axis. Whereas, the corresponding MPMDs at $t = 5.2$ optical cycles [Fig. 4(b2)] and $t = 7.3$ optical cycles [Fig. 4(c2)] both localizes mainly along the y axis with the small tilted angle which mainly comes from the resulting effects of the nonspherical molecular Coulomb potential and the helicity of the laser field with tilting in the same direction as the rotation of the laser field [16,21,34]. And our results of time evolution of MPMDs here confirm the theoretical interpretation well. In addition, as time evolves, the intensity of the MPMD becomes larger.

The research changing internuclear distance has been done by Li *et al.* [23] and Yuan *et al.* [32]; the results show that the phenomenon of LIED may occur by significantly changing the internuclear distance R. However, in our simulation here, the internuclear distance R is changed slightly around the equilibrium internuclear distance R_e. The MPMDs and time-propagation method, are shown in Figs. 3(a1)–3(a4) (from $R_1 = 1.9$ a.u. to $R_4 = 2.2$ a.u.). The distributions in these four figures all mainly locate at three regions with the highest intensity of distribution in the central region. And the distributions of weaker intensity in the other two regions are all distributed mainly along the x axis. As the internuclear distance increases, the intensity of distribution located at around $p_x = \pm 2$ a.u. gets higher and higher. The characteristics of the final MPMDs [in Figs. 1(b1) and 2(a1)–2(c1)] agree well with those of the initial MPMDs, indicating that the difference of initial molecular structure causes the change in the final MPMDs.

To further analyze the effect of R on MPMDs, the MPMDs under different internuclear distances at $t = 3.6$ optical cycles, $t = 5.2$ optical cycles, and $t = 7.3$ optical cycles are shown in Fig. 4. The MPMDs at different times shown in Figs. 4(a1)–4(a4), 4(b1)–4(b4), and 4(c1)–4(c4) present similar characteristics changing with increasing R, which agrees well with that of the initial and final MPMDs. The results show that it is the change of initial molecular structure that leads to the change in the final MPMDs.

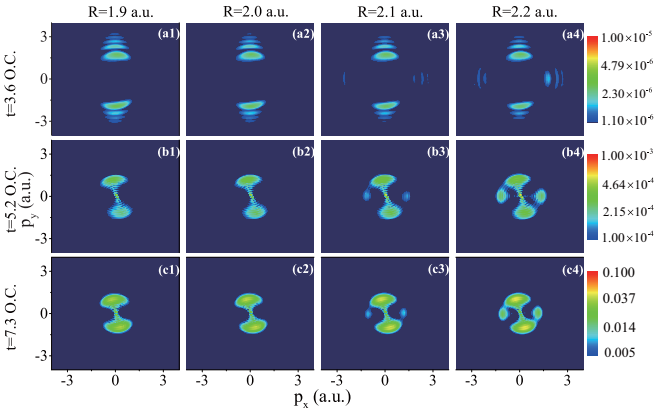

FIG. 4. The 2D MPMDs of aligned H_2^+ by elliptically polarized laser pulse ($\lambda = 30$ nm, $\varepsilon = 0.5$) with changing internuclear distance ($R = 1.9$ a.u. [(a1)–(c1)], 2 a.u. [(a2)–(c2)], 2.1 a.u. [(a3)–(c3)], and 2.2 a.u. [(a4)–(c4)]) at time $t = 3.6$ O.C. [(a1)–(a4)], 5.2 O.C. [(b1)–(b4)], and 7.3 O.C. [(c1)–(c4)], respectively. O.C. denotes the optical cycle.

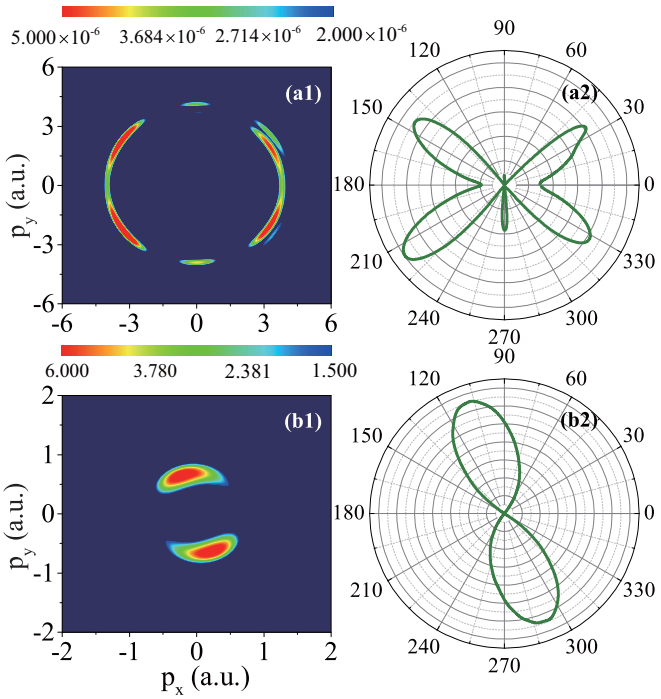

FIG. 5. The 2D MPMDs and MPADs of aligned H_2^+ at equilibrium $R_e = 2$ a.u. by elliptically polarized laser pulse with different wavelengths. The molecule is aligned along the x axis and the ellipticity is fixed at $\varepsilon = 0.5$. Wavelength is 5 nm (upper row) and 35 nm (bottom row). (a1)–(b1) and (a2)–(b2) are MPMDs and MPADs, respectively.

MPADs show the sensitivity on R that is subtly changed, which contains the information of molecular structures.

Figure 5 shows the λ dependence of MPMDs and MPADs. The wavelengths are chosen to be 5 nm ($\omega_1 = 9.11$ a.u.) and 35 nm ($\omega_2 = 1.30$ a.u.). Other parameters are the same as that in Fig. 2. For single-photon ionization, according to the energy conservation, the momentum of the ionized electron is $p_i = \sqrt{2(\omega_i - I_p)}$, with $p_1 = 4.00$ a.u. and $p_2 = 0.63$ a.u. And the corresponding de Broglie wavelengths of the ionized electron can be expressed as $\lambda_i = 2\pi/p_i$, which are $\lambda_1 = 1.57$ a.u. and $\lambda_2 = 9.90$ a.u., respectively.

The initial wave packet of H_2^+ is peaked equally at two indistinguishable nuclei that are separated by the internuclear distance R in Eq. (12) in Ref. [16]; the "cos" term is the interference of two outgoing wave functions, which is identical to the classical Young double-slit interference formula of optics [39].

The de Broglie wavelength ($\lambda_2 = 9.90$ a.u.) for 35 nm is greater than the equilibrium internuclear distance ($R_e = 2$ a.u.). $\cos(\mathbf{p}\cdot\mathbf{R}/2) = \cos[\mathrm{pR}\cos(\theta)/2]$, thus $pR/2 = \pi R/\lambda_2 < \pi$, which means that the maximum distribution satisfies the condition that $\cos(\theta) > 1$ at $\mathbf{p}\cdot\mathbf{R}/2 = \pi$. Then $\theta = \pi/2 \pm \pi$, lying along the y direction and showing no diffraction. For the 5 nm case, $pR/2 = \pi R/\lambda_1 = 1.27\pi$, and the maximum distribution satisfies $1.27\pi\cos(\theta) = n\pi$, $n = 0, \pm 1$. Thus, $\theta = \pm 90°, \pm 38°, \pm 142°$, which apparently shows the LIED pattern.

The research observing the LIED phenomenon has been done by others [23,32]; the phenomenon of LIED appears after changing significantly the internuclear distance R. In fact, the fundamental principle is the same in both the previous study (by changing internuclear distance) and this current study (by changing laser wavelength). The core is to weigh the relative scale between the de Broglie wavelength of photoelectrons and the internuclear distance of molecules. The above interpretations explain the complex MPMDs and MPADs well in Fig. 5.

IV. CONCLUSIONS

In summary, we study the MPMD and MPAD of aligned H_2^+ driven by an elliptically polarized laser pulse by means of numerically solving 2D TDSE under frozen-nuclei approximation. The MPMDs and MPADs show the dependence on the varying ellipticity of the laser. We then change the internuclear distance with fixed ellipticity; the results show that the MPMDs and MPADs are sensitive to the internuclear distance. The initial MPMDs and the evolution of MPMDs are presented to interpret the dependence of MPMDs on R. The phenomenon, which is called LIED, occurs when the wavelength of the laser changes from 35 to 5 nm. The attosecond perturbation ionization theory and exactly solvable photoionization model are employed to interpret the results above.

ACKNOWLEDGMENTS

This work was partially supported by National Natural Science Foundation of China under Grants No. 11574117 and No. 61575077, National Defense Pre-Research Foundation of China under Grant No. 419140100048, and Natural Science Foundation of Jilin Province of China under Grant No. 20180101225JC.

[1] T. Brabec and F. Krausz, Rev. Mod. Phys. **72**, 545 (2000).
[2] F. Krausz, Rev. Mod. Phys. **81**, 163 (2009).
[3] E. Goulielmakis, Z. Loh, A. Wirth, R. Santra, N. Rohringer, V. S. Yakovlev, S. Zherebtsov, T. Pfeifer, A. M. Azzeer, M. F. Kling, S. R. Leone, and F. Krausz, Nature (London) **466**, 739 (2010).
[4] S. Haessler, J. Caillat, W. Boutu, C. Giovanetti-Teixeira, T. Ruchon, T. Auguste, Z. Diveki, P. Breger, A. Maquet, B Carré, R. Taïeb, and P. Salières, Nat. Phys. **6**, 200 (2010).
[5] J. Mauritsson, T. Remetter, M. Swoboda, K. Klünder, A. L'Huillier, K. J. Schafer, O. Ghafur, F. Kelkensberg, W. Siu, P. Johnsson, M. J. J. Vrakking, I. Znakovskaya, T. Uphues, S. Zherebtsov, M. F. Kling, F. Lépine, E. Benedetti, F. Ferrari, G. Sansone, and M. Nisoli, Phys. Rev. Lett. **105**, 053001 (2010).
[6] P. Tzallas, E. Skantzakis, L. A. A. Nikolopoulos, G. D. Tsakiris, and D. Charalambidis, Nat. Phys. **7**, 781 (2011).
[7] A. D. Bandrauk and S. Chelkowski, Chem. Phys. Lett. **336**, 518 (2001).
[8] T. Zuo, A. D. Bandrauk, and P. B. Corkum, Chem. Phys. Lett. **259**, 313 (1996).
[9] M. Meckel, D. Comtois, D. Zeidler, A. Staudte, D. Pavičić, H. C. Bandulet, H. Pépin, J. C. Kieffer, R. Dörner, D. M. Villeneuve, and P. B. Corkum, Science **320**, 1478 (2008).

[10] C. I. Blaga, J. Xu, A. D. Dichiara, E. Sistrunk, K. Zhang, P. Agostini, T. A. Miller, L. F. DiMauro, and C. D. Lin, Nature (London) **483**, 194 (2012).
[11] J. Li, X. Ren, Y. Yin, K. Zhao, A. Chew, Y. Cheng, E. Cunningham, Y. Wang, S. Hu, Y. Wu, M. Chini, and Z. Chang, Nat. Commun. **8**, 186 (2017).
[12] T. Gaumnitz, A. Jain, Y. Pertot, M. Huppert, I. Jordan, F. Ardana-Lamas, and H. J. Wörner, Opt. Express. **25**, 27506 (2017).
[13] M. Murakami and Shih-I Chu, Phys. Rev. A **93**, 023425 (2016).
[14] W. Y. Wu and F. He, Phys. Rev. A **93**, 023415 (2016).
[15] K. Yuan, H. Lu, and A. D. Bandrauk, Struct. Chem. **28**, 1297 (2017).
[16] K. Yuan, S. Chelkowski, and A. D. Bandrauk, Chem. Phys. Lett. **638**, 173 (2015).
[17] D. M. Villeneuve, P. Hockett, M. J. J. Vrakking, and H. Niikura, Science **356**, 1150 (2017).
[18] X. Xie, T. Wang, S. G. Yu, X. Y. Lai, S. Roither, D. Kartashov, A. Baltuška, X. J. Liu, A. Staudte, and M. Kitzler, Phys. Rev. Lett. **119**, 243201 (2017).
[19] C. A. Mancuso, D. D. Hickstein, K. M. Dorney, J. L. Ellis, E. Hasović, R. Knut, P. Grychtol, C. Gentry, M. Gopalakrishnan, D. Zusin, F. J. Dollar, X. M. Tong, D. B. Milošević, W. Becker, H. C. Kapteyn, and M. M. Murnane, Phys. Rev. A **93**, 053406 (2016).
[20] M. Odenweller, J. Lower, K. Pahl, M. Schütt, J. Wu, K. Cole, A. Vredenborg, L. Ph. Schmidt, N. Neumann, J. Titze, T. Jahnke, M. Meckel, M. Kunitski, T. Havermeier, S. Voss, M. Schöffler, H. Sann, J. Voigtsberger, H. Schmidt-Böcking, and R. Dörner, Phys. Rev. A **89**, 013424 (2014).
[21] M. Odenweller, N. Takemoto, A. Vredenborg, K. Cole, K. Pahl, J. Titze, L. Ph. H. Schmidt, T. Jahnke, R. Dörner, and A. Becker, Phys. Rev. Lett. **107**, 143004 (2011).
[22] H. D. Cohen and U. Fano, Phys. Rev. **150**, 30 (1966).
[23] Y. Li, M. Qin, X. Zhu, Q. Zhang, P. Lan, and P. Lu, Opt. Express. **23**, 10687 (2015).
[24] T. T. Nguyen-Dang, M. Peters, J. Viau-Trudel, E. Couture-Bienvenue, R. Puthumpally-Joseph, E. Charron, and O. Atabek, Mol. Phys. **115**, 1934 (2017).
[25] R. Puthumpally-Joseph, J. Viau-Trudel, M. Peters, T. T. Nguyen-Dang, O. Atabek, and E. Charron, Mol. Phys. **115**, 1889 (2017).
[26] J. A. You, J. M. Dahlström, and N. Rohringer, Phys. Rev. A **95**, 023409 (2017).
[27] J. W. Geng, L. Y. Peng, S. N. Song, and Q. Gong, Phys. Rev. A **88**, 053418 (2013).
[28] C. Serrat, Phys. Rev. Lett. **111**, 133902 (2013).
[29] S. Cui, P. L. He, and F. He, Phys. Rev. A **94**, 053401 (2016).
[30] L. Peng, E. A. Pronin, and A. F. Starace, New. J. Phys. **10**, 025030 (2008).
[31] J. M. N. Djiokap, S. Hu, W. Jiang, L. Peng, and A. F. Starace, New. J. Phys. **14**, 095010 (2012).
[32] K. J. Yuan, H. Z. Lu, and A. D. Bandrauk, Phys. Rev. A **83**, 043418 (2011).
[33] P. L. He, N. Takemoto, and F. He, Phys. Rev. A **91**, 063413 (2015).
[34] K. Yuan, S. Chelkowski, and A. D. Bandrauk, Chem. Phys. Lett. **592**, 334 (2014).
[35] D. Akoury, K. Kreidi, T. Jahnke, Th. Webery, A. Staudte, M. Schöffler, N. Neumann, J. Titze, L. Ph. H. Schmidt, A. Czasch, O. Jagutzki, R. A. Costa Fraga, R. E. Grisenti, R. Díez Muiño, N. A. Cherepkov, S. K. Semenov, P. Ranitovic, C. L. Cocke, T. Osipov, H. Adaniya, J. C. Thompson, M. H. Prior, A. Belkacem, A. L. Landers, H. Schmidt-Böcking, and R. Dörner, Science **318**, 949 (2007).
[36] E. A. Pronin, A. F. Starace, M. V. Frolov, and N. L. Manakov, Phys. Rev. A **80**, 063403 (2009).
[37] E. A. Pronin, A. F. Starace, and L. Y. Peng, Phys. Rev. A **84**, 013417 (2011).
[38] M. D. Girardeau, K. G. Kim, and C. C. Widmayer, Phys. Rev. A **46**, 5932 (1992).
[39] N. H. Franck, *Introduction to Electricity and Optics* (McGraw-Hill, New York, 1940).